Journal of the European Ceramic Society 23 (2003) 1105–1114

www.elsevier.com/locate/jeurceramsoc

Creep behaviour of a SiC/Si-B-C composite with a self-healing multilayered matrix

Philippe Carrère, Jacques Lamon*

Laboratoire des Composites Thermostructuraux, UMR 5801(CNRS-Snecma-CEA-Université Bordeaux 1), 3, Allée de La Boétie, 33600 Pessac, France

Received 12 January 2002; received in revised form 2 July 2002; accepted 14 July 2002

Abstract

The creep behaviour of a SiC/Si-B-C composite at 1200 °C in argon is investigated under static and cyclic loading conditions. The SiC/Si-B-C composite consists of a multilayered self healing matrix reinforced with Nicalon fibers. It was produced via chemical vapor infiltration (CVI). The creep behaviour is examined with respect to the extent of damage created during an initial step of monotonic loading and controlled through the applied strain. The creep rate is shown to be dictated mainly by creep of fibers and interfacial debonding, whereas no significant creep induced matrix cracking was detected.
© 2002 Elsevier Science Ltd. All rights reserved.

Keywords: Ceramic matrix composites; Creep; Damage; Fatigue; Multilayers; SiC/SiC

1. Introduction

Ceramic matrix composites reinforced with long fibers are potential candidates for use in aerospace industry, under severe conditions of temperatures and environment. The SiC/SiC composites consisting of a SiC matrix reinforced using SiC fibers display some favorable characteristics such as high mechanical properties and a good resistance to high temperatures. SiC/SiC composites exhibit a certain sensitivity to interfacial degradation by oxidation at temperatures above 450 °C. In order to protect the PyC interphase against oxidation effects, SiC/Si-B-C composites with a multilayered matrix have been developed[1] and investigated.[2–5] Such multilayered matrices contain phases which produce sealants at high temperatures causing healing of the cracks and preventing oxygen from reaching the interphase. The fatigue behaviour has been investigated at temperatures as high as 1200 °C.[2–5] At temperatures above 1100 °C, crack healing, limited damage and creep were evidenced.[5]

Creep of ceramic matrix composites involves stress transfers between the matrix and the fibers caused by their differing creep rates, that may lead to fiber failures or matrix cracking followed by debonding and sliding at the interfaces.[6–8] When the matrix is elastic and creep resistant, fiber creep induces stress transfer from the fibers onto the matrix that may cause matrix cracking. This matrix damage has been observed on SiC/SiC.[9–12] In these materials the SiC matrix is far more creep resistant than the Nicalon fiber, which is unstable and creeps at 1100 °C.[9,13,14] At this stage, there are no data available on the creep resistance of the Si-B-C matrix.

When the SiC/Si-B-C composite is tested in air, the combined contributions of creep and oxidation above 1100 °C make difficult the analysis of creep behaviour. The present paper investigates the creep behaviour of a SiC/Si-B-C composite at 1200 °C in argon. Lower temperatures have been disregarded since the creep effects would not have been significant enough. For comparison purposes the creep behaviour of SiC/SiC composites was also examined.

2. Experimental

2.1. Materials

The 2D-SiC/Si-B-C composite (Fig. 1a) was produced via chemical vapor infiltration by SNECMA Moteurs

* Corresponding author. Tel.: +33-556-844-703; fax: +33-556-841-225.

E-mail address: lamon@lcts.u-bordeaux.fr (J. Lamon).

0955-2219/03/$ - see front matter © 2002 Elsevier Science Ltd. All rights reserved.
PII: S0955-2219(02)00273-X

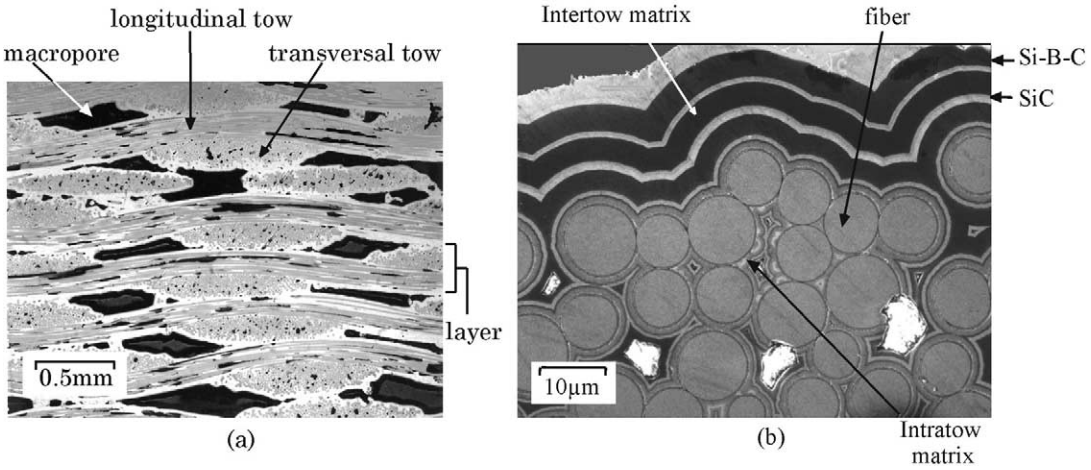

Fig. 1. Scanning electron microscopy micrographs showing the structure of the Si-B-C composite (a), and the multilayer matrix (b).

(France). It consists of a multilayered matrix (Fig. 1b) and plies of woven tows of SiC fibers (Nicalon NL 202) (Fig. 1b). The fibers were coated with a thin layer of pyrocarbon deposited via CVI. The matrix contains phases of the Si-B-C ternary system.

2.2. Creep tests

The creep apparatus (Fig. 2) consists essentially of an induction heated furnace mounted on an electro-mechanical tensile testing machine. The furnace and the grips are located within a hermetic chamber which can be evacuated and then filled with argon or nitrogen.

The test specimens were held by water cooled grips. The test temperature is uniform along the central part of the specimens (25 mm), which coincides with the gauge length for measurement of deformations using a contact extensometer. The temperature was monitored using two thermocouples and a pyrometer (Fig. 2).

All the specimens were tested at 1200 °C in argon (pressure 500 kPa). They were heated first to the test temperature at a rate of 50 °C/min. Loading started

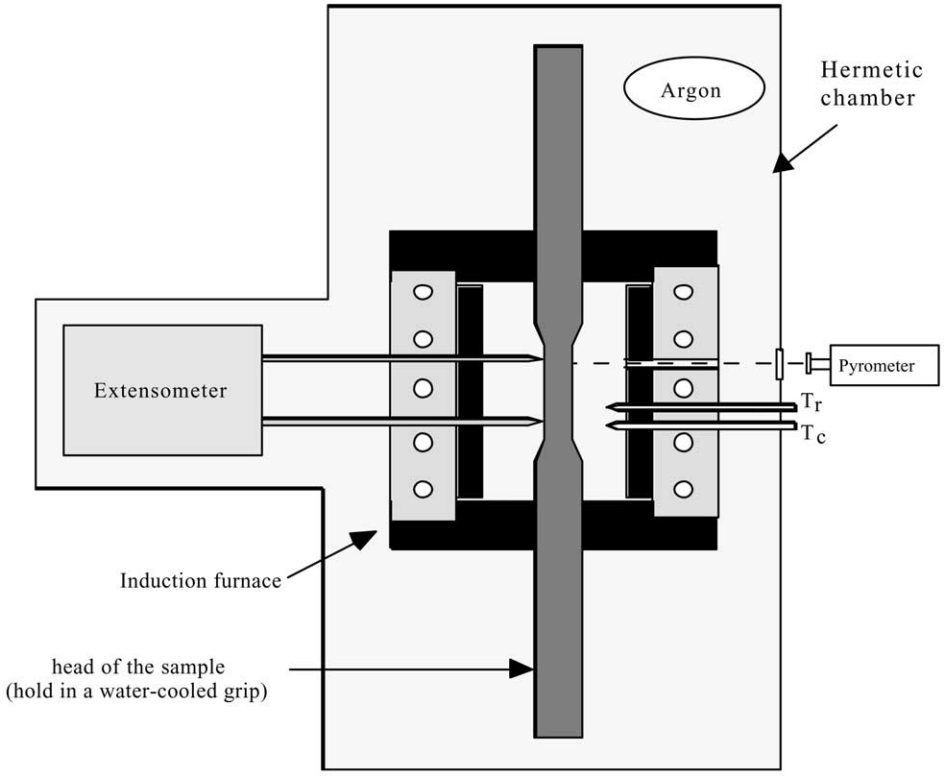

Fig. 2. Creep test apparatus.

only 1 h after the test temperature was reached, so that the temperature was uniform over the gauge length.

In a first step, the specimens were loaded monotonically (stress rate = 100 MPa/min) to a given strain ε_0 (Fig. 3), then unloaded. This first cycle was aimed at creating controlled damage in the matrix according to the following sequence evidenced in previous works[2,3,15] and summarized in Table 1:

- when $\varepsilon_0 \leqslant 0.3\%$, damage results from cracks located in the interply matrix and in the transverse tows,
- when $\varepsilon_0 \geqslant 0.3\%$, damage results from microcracks located in the matrix of longitudinal tows.

Then the load was *smaller than that applied during the first damage cycle*. It was either constant (static fatigue) or time dependent (cyclic fatigue, frequency 1 Hz) (Table 2).

The elastic modulus E was measured after the first damage cycle and then periodically, during an unloading—reloading cycle at a stress-rate of 400 MPa/mn (Fig. 3). The elastic modulus was derived from the final linear portion of the stress–strain curve on reloading:minimum tangent modulus.[2,5] This straight line generally intercepts the origin.

Static fatigue tests were also performed on two SiC/SiC specimens (Table 2), for comparison purposes.

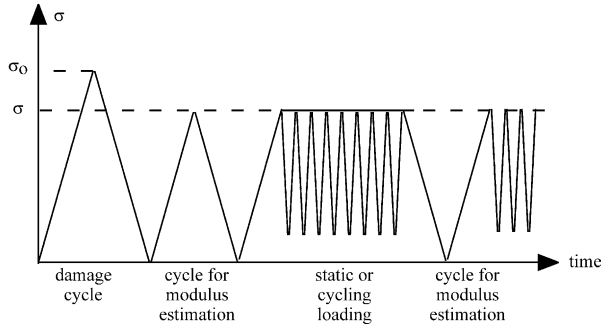

Fig. 3. Loading procedure during the static and cyclic fatigue tests at 1200 °C.

Table 1
Densities of cracks in the intertow matrix and in the transverse tows with respect to temperature and applied load (stress and deformation)[a]

T (°C)	σ (MPa)	ε_0 (%)	Density of cracks in intertow matrix (%)	Density of cracks in transverse tows (%)
20	106	0.05	50	15
20	162	0.12	100	60
1200	100	0.05	10	30
1200	150	0.12	50	75
1200	200	0.3	100	100

[a] When $\varepsilon_0 \geqslant 0.3\%$, matrix cracks appear within the longitudinal tows oriented parallel to the loading direction.

All the tests were interrupted before ultimate failure. After cooling down at a rate of 50 °C/min, the test specimens were cut and polished on the lateral face for examination using an optical microscope.

3. Results

3.1. Creep of the SiC/Si-B-C composite in static fatigue

Typical creep curves are shown on Figs. 4 and 5. Secondary creep was not observed, even during long duration tests (85 h). The creep rate decreased steadily (Fig. 6). A log–log plot of creep rate versus time shows that, after a certain time t_0 (generally longer than 1 h), the creep rate data closely fit the following equation for $n = -0.8$:

$$\mathrm{Ln}\dot{\varepsilon} = n\mathrm{Ln}\frac{t}{t_0} + \ln A \quad (1)$$

where A is a constant, and t_0 a time scale factor. t_0 was taken to be 1 h.

Table 2
Experimental conditions for the creep tests at 1200 °C under argon

Composite	Loading	ε_0 (%)	Applied stress (MPa)	R
SiC/Si-B-C	Static	0.15	100	
		0.2	100	
		0.25	100	
		0.25	150	
		0.5	100	
		0.8	60	
		0.8	100	
		0.8	150	
SiC/Si-B-C	Cyclic	0.1	100	0.1
		0.25	130	0.5
		0.25	150	0.2
SiC/SiC	Static	0.14	150	
		0.22	150	

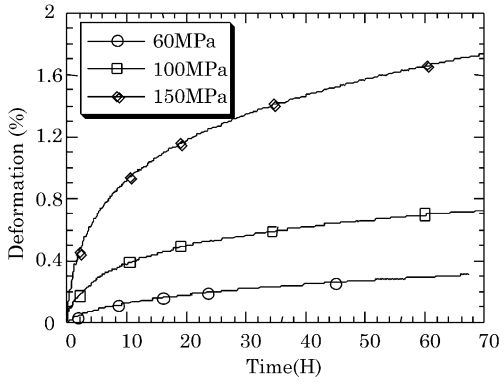

Fig. 4. Creep curves under static fatigue at 1200 °C ($\varepsilon_0 = 0.8\%$) for various applied stresses.

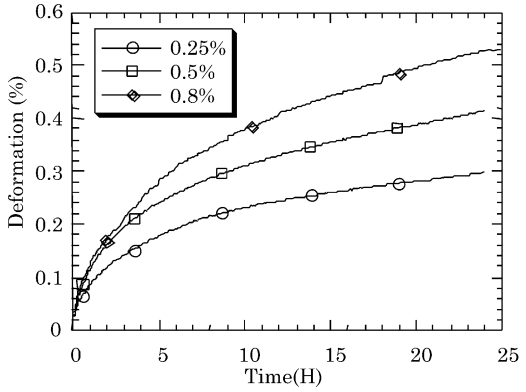

Fig. 5. Creep curves under static fatigue (applied stress 100 MPa at 1200 °C) for various damage strains ε_0.

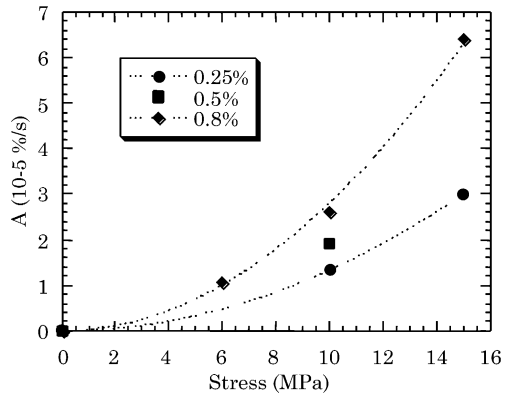

Fig. 7. Values of constant A versus applied stress for various damage strains ε_0.

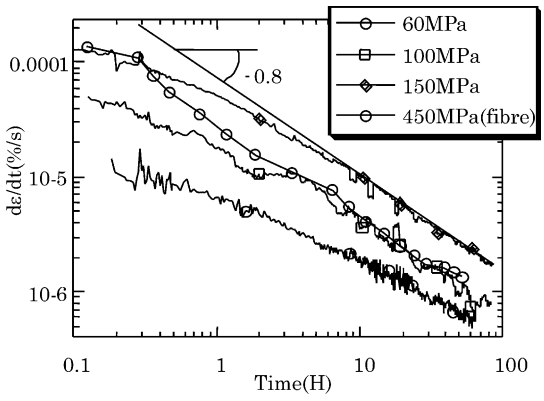

Fig. 6. Creep rate curves for a damage strain $\varepsilon_0 = 0.8\%$ and for various applied constant stresses for the SiC/Si-B-C composite, and under 450 MPa at 1200 °C in argon for a Nicalon NL202 fiber.[17]

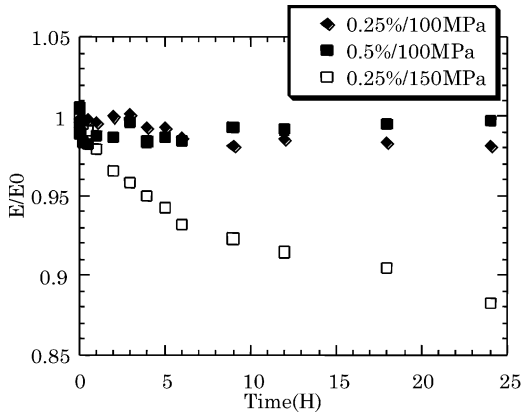

Fig. 8. Evolution of elastic modulus during the static fatigue tests at 1200 °C.

Eq. (1) implies that $\dot{\varepsilon}(t) = A(t/t_0)^n$ (2)

This empirical equation has no physical meaning, but it provides a convenient model of primary creep rate. Table 2 shows that A increases with the applied stress σ, and with the initial damage (ε_0). Fig. 7 shows that the stress dependence of A is described by the following equation:

$$A = B(\varepsilon_0).\sigma^2 \quad (3)$$

where $B(\varepsilon_0)$ is an initial damage dependent parameter.

Fig. 5 shows that deformations remained smaller than 0.3% when $\varepsilon_0 \leqslant 0.25\%$. Larger deformations were measured only when $\varepsilon_0 > 0.3\%$, i.e. when initial damage involved cracks located in the longitudinal tows. It can be noticed that strains were quite large when $\varepsilon_0 = 0.8\%$, i.e. when matrix cracking in the longitudinal tows reaches the saturation point.

Fig. 8 and Table 3 indicate that the elastic modulus decreased only when $\varepsilon_0 < 0.25\%$. The modulus variations are small suggesting that damage induced creep was limited. By contrast, when $\varepsilon_0 > 0.25\%$, the elastic modulus remained constant suggesting that matrix damage did not develop.

Optical microscopy on the lateral faces of test specimens revealed that the cracks were located in the intertow matrix and in the transverse tows of those specimens initially damaged under $\varepsilon_0 = 0.2\%$, and that they were widely opened (Fig. 9). Significant debonding of the tows can be noticed (Fig. 9). Cracks were not detected within the longitudinal tows when $\varepsilon_0 \leqslant 0.25\%$.

Data in Table 3 indicate a dependence of crack spacing distance on initial damage: 300, 200 and 100 μm were measured respectively for $\varepsilon_0 = 0.25$, 0.5 and 0.8%. These values are similar to those measured on specimens that had been subjected to monotonic loading at room and at high temperatures. The results indicate that the possible creep induced matrix damage was not significant.

Table 3
Main features of the behaviour of the SiC/Si-B-C composites under static and cyclic fatigue at 1200 °C in argon[a]

ε_0 (%)	σ (MPa)	R	A (10^{-5} %/s)	$\Delta E/E$ (%)	l_s (μm)
0.15	100	Static	1.3	−13	–
0.2	100	figure	1.5	−11	–
0.25	100		1.35	0	297
0.25	150		3	−12	300
0.5	100		1.9	0	209
0.8	60		1.05	0	–
0.8	100		2.6	0	105
0.8	150		6.4	0	99
0.1	100	0.1	0.35	−6	315
0.25	130	0.5	0.84	−6	220
0.25	150	0.2	0.85	−20	210

[a] $\Delta E/E$ is the elastic modulus variation during the tests ($\Delta E = E_F - E(\varepsilon_0)$, where E_F is the elastic modulus at the end of the tests, and $E_0(\varepsilon_0)$ that one after the first damage cycle), l_s is the spacing distance for the transverse cracks.

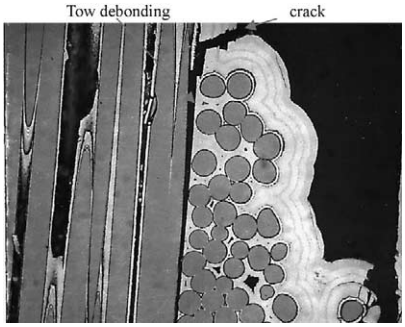

Fig. 9. Optical micrograph of a SiC/Si-B-C composite initially damaged under $\varepsilon_0 = 0.2\%$ and tested during 100 h in static fatigue under 100 MPa at 1200 °C.

3.2. Creep of the SiC/Si-B-C composites under cyclic fatigue

As previously in static fatigue, the strain-time behaviour reveals essentially a primary creep (Figs. 10 and 11). The creep rate data again fit closely Eq. (1) with $n = -0.8$ (Fig. 11). The values of A reported in Table 3 are smaller than those obtained under static loading, indicative of a slower creep rate under cyclic loading.

Fig. 10 shows that deformations exceeded slightly 0.3% under 150 MPa, whereas they remained smaller than 0.3% when 100 MPa was applied.

The elastic modulus decreases were limited, except for that specimen subject to 150 MPa. Optical microscopy revealed the presence of matrix cracks within longitudinal tows in this particular specimen (Fig. 12). Since $\varepsilon_0 < 0.3\%$, these cracks were probably not present after the first damage cycle. They may have been created during the fatigue tests.

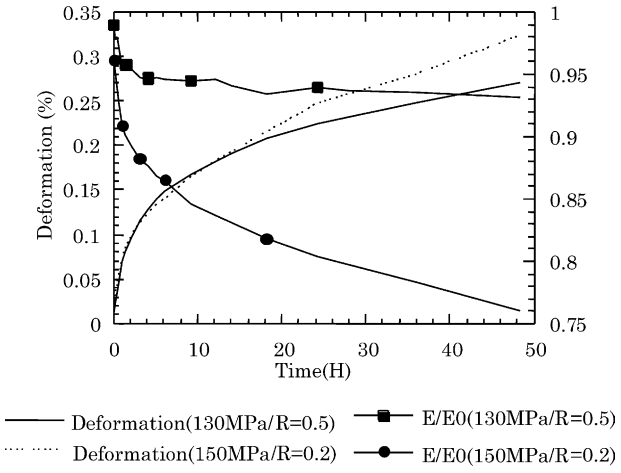

Fig. 10. Creep curves and elastic modulus variations under cyclic loading at 1 Hz and for $\varepsilon_o = 0.25\%$ at 1200 °C.

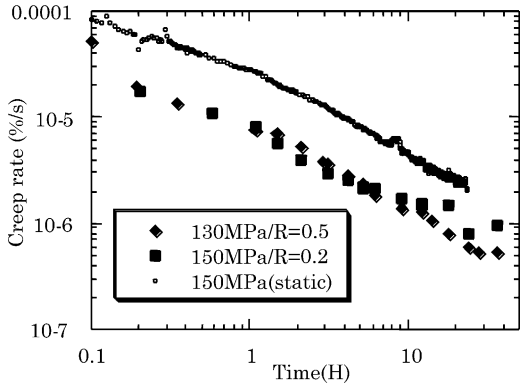

Fig. 11. Creep rate curves under cyclic and static loading for $\varepsilon_0 = 0.25\%$ at 1200 °C.

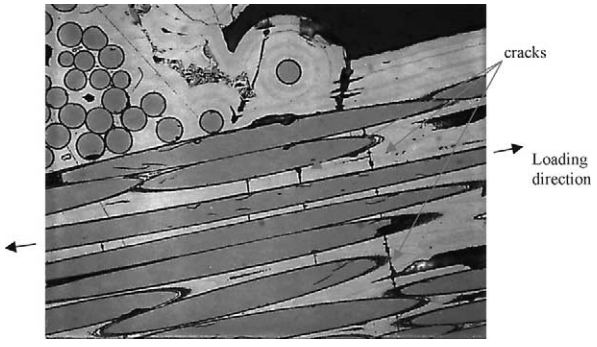

Fig. 12. Optical micrograph of a SiC/Si-B-C composite initially damaged under $\varepsilon_0 = 0.25\%$ and tested under cyclic loading (maximum stress = 150 MPa) at 1200 °C.

3.3. Creep of the SiC/SiC composites under static fatigue

Fig. 13 shows that the creep rate decreases steadily and that the trend is comparable to that described by Eq. (2) but the time exponent is larger than −0.8 and

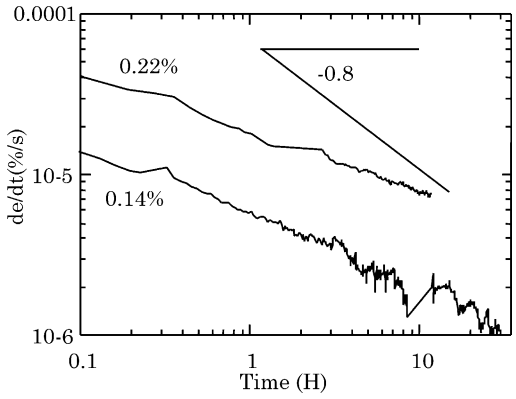

Fig. 13. Creep rate curves for the SiC/SiC composite under a constant stress of 150 MPa ($\varepsilon_0 = 0.14$ and $\varepsilon_0 = 0.22\%$) at 1200 °C.

increasing with ε_0 (Table 4). This suggests a different creep mechanism.

A significant modulus decrease was measured after the tests (Table 4). A dense microcracking was observed within the longitudinal tows, although the damage strain was $\varepsilon_0 \leqslant 0.22\%$, which indicates that the cracks were created or propagated during the static fatigue tests.

4. Discussion

4.1. Creep mechanisms

It has been shown in other works[3,5,16] that the applied load is carried by the fibers only (those parallel to the loading direction) beyond the matrix cracking saturation strain ($\varepsilon_0 = 0.8\%$), as a result of complete debonding. Therefore, it may be expected that the creep behaviour is dictated by the fibers in those composites which experienced such damage ($\varepsilon_0 \geqslant 0.8\%$). However, creep of fibers within the composite may be influenced by undulations and by a specific confined environment.

Indeed, the creep rate of those specimens initially subjected to $\varepsilon_0 = 0.8\%$ displays the same time dependence as that of Nicalon fibers in various atmospheres:[17] Nicalon fibers exhibit primary creep only, at 1200 °C and the time exponent is also $n = -0.8$ (Fig. 6). The absence of secondary creep in Nicalon fibers was attributed to growth of the SiC grains which increases the creep resistance.[14,17]

Table 4
Results of the creep tests on the SiC/SiC composites

ε_0 (%)	σ (MPa)	$\Delta E/E$ (%)	t (h)	A (10^{-5} %/s)	n
0.14	150	– 36	30	0.6	– 0.56
0.22	150	– 40	12	2	– 0.4

Since exactly the same time dependence of creep rate was observed on the other specimens with a less severe initial damage ($\varepsilon_0 < 0.8\%$), it is reasonable to think that their creep behaviour was also controlled by the fibers. Furthermore, it can be noticed from Fig. 5 that deformations were larger as initial matrix damage was more significant, i.e., as the contribution of fiber elongation in composite deformation increased. Very few cracks were detected in the longitudinal tows when $\varepsilon_0 \leqslant 0.25\%$. The overall deformation remained in agreement with the initial extent of matrix damage, i.e. it remained smaller than 0.3% (Fig. 5). However the cracks in the intertow matrix and in the transverse tows were widely opened and they were associated to significant tow debonding (Fig. 9). This feature indicates large local deformations of longitudinal tows. This suggests that creep of both the fibers and the matrix occurred within the longitudinal tows that were debonded from the intertow matrix. Creep of the intratow matrix is possible since it consists of nanometer size SiC grains within an amorphous phase.[2] By contrast, creep of the intertow matrix is more difficult, since this matrix is composed of thick layers of well-crystallized SiC.

The small elastic modulus decreases which have been measured after the creep tests reflect the limited creep induced damage observed using optical microscopy. They may be attributed to debonding of the longitudinal tows.

Basically, the time exponent $n = -0.8$ was also determined under cyclic loading, suggesting that the previously discussed fiber-controlled creep mechanism operated. The modulus decrease was also comparable to that determined under static loading, suggesting the presence of a similar creep induced damage. However, values of constant A show that the creep rate was smaller when comparing to static fatigue results.

The SiC matrix is known to be very stiff and more creep resistant than the Nicalon fibers.[13,18] Thus, the SiC matrix cracks to accommodate the deformations induced by creep of fibers. The significant elastic modulus decreases determined for the SiC/SiC composite reflect this phenomenon.

The elastic modulus of Si-B-C is smaller than that of SiC (respectively 350 and 410 GPa). As a consequence, the Si-B-C matrix is subject to lower stresses than the SiC matrix does. Furthermore, it should be able to better accommodate elastically the deformations induced by the creeping fibers. Fig. 14 summarizes the mechanisms that contribute to creep in SiC/Si-B-C composites.

4.2. Creep behaviour of fiber within the composite with saturated matrix damage

If creep of composites with saturated matrix damage is dictated by the fibers, the creep behaviour of fibers can be derived from the creep curves determined on

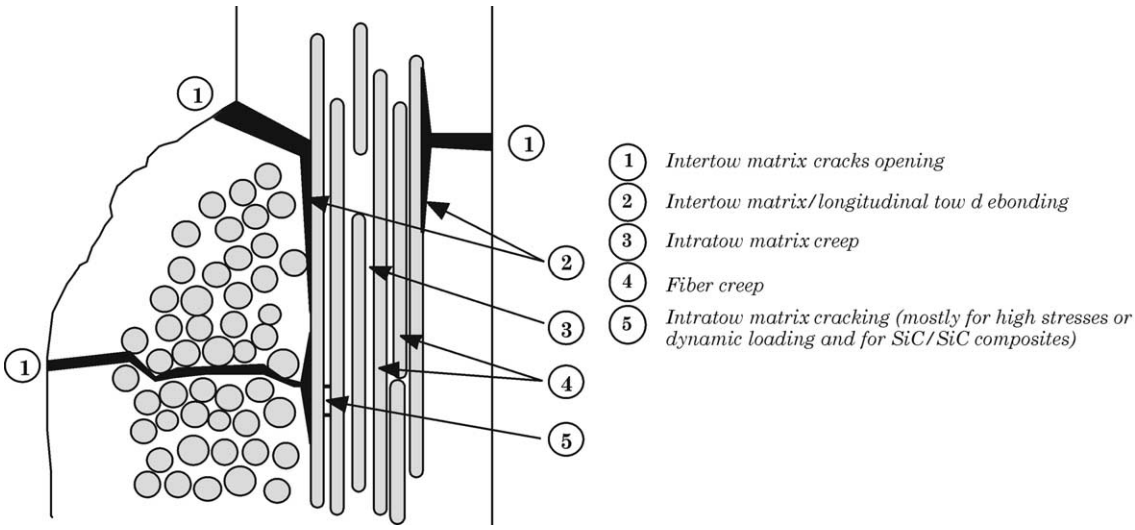

Fig. 14. Schematic diagram illustrating the mechanisms involved in the creep behaviour of SiC/Si-B-C composite.

these composites subject to a damage strain $\varepsilon_0 = 0.8\%$. Assuming that the load is carried by the longitudinal fibers only[2,5,16] and neglecting the effect of weaving, the stress (σ_f) operating on the fibers is related to the stress (σ) applied to the composite by the following equation:

$$\sigma_f = \frac{2\sigma}{V_f} \tag{4}$$

Incorporating the expression of σ into (2) gives the following creep law at 1200 °C for the fiber (for times longer than 10 h):

$$\dot{\varepsilon} = B_f \left(\frac{t}{t_0}\right)^{-0.8} \sigma_f^2 \tag{5}$$

where $B_f = \frac{B(0.8)V_f^2}{4} = 10^{-8}\%\ \mathrm{s}^{-1}\ \mathrm{MPa}^{-2}$.

It is interesting to compare these results with creep data determined on Nicalon fibers tested individually. Bodet and coworkers[17] have investigated the creep behaviour of Nicalon fibers in argon and in CO atmospheres. They found that the fibers exhibit only primary creep at 1200 °C and they obtained similar creep curves under argon and under argon/CO atmospheres.

Fig. 6 compares the creep curves determined on a Nicalon fiber under $\sigma_f = 450$ MPa and on the composite. It can be noticed that the fiber creep behaviour coincides satisfactorily to that of the specimen tested under $\sigma = 100$ MPa. This typical stress corresponds to $\sigma_f = 450$ MPa through Eq. (4). Furthermore, Eq. (5) fits the fiber experimental data obtained under 450 MPa for $B_f = 1.5\ 10^{-8}\ \%\ \mathrm{s}^{-1}\ \mathrm{MPa}^{-2}$. This B_f estimate is quite close to the above value derived from the composite creep rate.

Bodet and coworkers[17] found that the creep rate is proportional to the stress (stress exponent = 1). Di Carlo and Yun also mentioned the same stress exponent for the Nicalon fiber.[19] The primary creep of Nicalon fibers was attributed to microstructural evolution (grain growth and decomposition).[14] When the fiber is confined within a composite, no decomposition into gaseous species is possible which limits its degradation. For the more stable Hi-Nicalon fiber, Bodet and Di-Carlo found a stress exponent close to 2, similar to that appearing in Eqs. (3) and (5). Therefore it may be concluded that the differences observed in creep rate stress dependence for Nicalon fibers tested individually or within a SiC/Si-B-C composite are mainly due to an enhanced stability when they are sheathed by the Si-B-C matrix.

4.3. Creep behaviour of the fiber in the presence of unsaturated matrix damage

For a first approximation, let's consider that the composite can be represented by an equivalent unidirectional composite consisting of a single fiber embedded in a matrix (Fig. 15). This simple model is aimed essentially at evaluating of the contribution of fiber creep and debonding to the overall creep behaviour. The creep rate of the composite is given by:

$$\dot{\varepsilon} = \dot{\varepsilon}_1 \frac{L_o - L_d}{L_o} + \dot{\varepsilon}_2 \frac{L_d}{L_o} \tag{6}$$

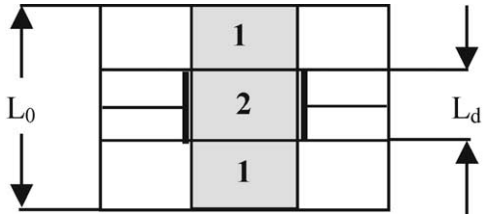

Fig. 15. Schematic diagram showing the equivalent unidirectional damaged composite.

where $\dot{\varepsilon}_1$ and $\dot{\varepsilon}_2$ are the creep rates in regions 1 and 2 respectively (Fig. 15).

Stresses on the fibers in region 2 (σ_2) where debond from the matrix is complete, are much larger than those in region 1 (σ_1)

$$\frac{\sigma_2}{\sigma_1} = \frac{2E_o}{V_f E_f} \cong 6 \tag{7}$$

where E_o is the elastic modulus of undamaged composites.

Therefore it can be assumed that creep in region 1 can be neglected and that the creep rate is controlled by region 2 where the debond is complete and high stresses prevail. Region 2 includes a portion where the stress decreases steadily from maximum in the region of fiber completely debonded from the matrix. In this intermediate portion, the creep rate is given by the following equation:[20]

$$\dot{\varepsilon} = \frac{\dot{\sigma_2'}}{E_f} + C\dot{\varepsilon}_2 \tag{8}$$

where E_f is the fiber elastic modulus, $\dot{\sigma}'_2$ is the stress, C is a time dependent coefficient.[20]

In the presence of a creep resistant matrix $\dot{\sigma}'_2$ can be neglected. Therefore, creep rate in the debonded region is controlled by fiber creep rate $\dot{\varepsilon}_2$.

Creep rate reduces to:

$$\dot{\varepsilon} = \alpha\dot{\varepsilon}_2 = \alpha B_f \left(\frac{t}{t_0}\right)^{-0.8} \left(\frac{2\sigma}{V_f}\right)^2 \tag{9}$$

where α represents the fraction of completely debonded fiber.

This value of α slightly underestimates the contribution of $\dot{\varepsilon}_2$ in composite creep. However, it can be noticed that the time exponent is $n=-0.8$, even when the contribution of creep in the intermediate region is taken into account.

α was estimated from the composite creep behaviour using Eq. (9) (referred to as α_1). It was compared to those values provided by composite elastic modulus (referred to as α_2):

$$\frac{1}{E} = \frac{1-\alpha}{E_0} + \frac{2\alpha}{E_f V_f} \tag{10}$$

Table 5 shows that α_1 and α_2 are very close when $\varepsilon_0 \geqslant 0.25\%$, which indicates that creep of the composite is dictated by creep of the fiber in the debonded region when the extent of damage is significant.

By contrast, $\alpha_1 > \alpha_2$ when $\varepsilon_0 \leqslant 0.25\%$ indicating that the effect of creep in region 2 was overestimated. This means that creep of debonded fibers is not the main mechanism involved in composite deformations. Additional elastic deformations can result from progressive debonding induced by creep of fibers in the completely debonded region. These results agree with the elastic modulus decreases that were obtained only for $\epsilon_0 \leqslant 0.25\%$ (Table 2).

Table 5
Comparison of α_1 and α_2 obtained for static fatigue tests

ε_0 (%)	σ (MPa)	α_1 [Eq. (9)]	α_2 [Eq. (10)]
0.15	100	0.47	0.27
0.2	100	0.54	0.40
0.25	100	0.49	0.35
0.25	150	0.48	0.43
0.5	100	0.69	0.65
0.8	60	1.00	1.00
0.8	100	0.94	1.00
0.8	150	1.03	1.00

Eq. (11) derived from Eq. (9) shows that a good fit to the experimental data shown on Fig. 11 can be obtained only when α is time undependent:

$$\mathrm{Ln}\dot{\varepsilon} = \mathrm{Ln}\alpha - 0.8\mathrm{Ln}\left(\frac{t}{t_0}\right) + \mathrm{Ln}\left[B_f\left(\frac{2\sigma}{V_f}\right)^2\right] \tag{11}$$

when α is constant, the slope of the Ln$\dot{\varepsilon}$-Lnt curve corresponds to the time exponent n. When α is time dependent, neither Ln$\dot{\varepsilon}$ is proportional to Lnt nor the slope of the curve is given by exponent $n=-0.8$.

This result helps in understanding the trends in strain rate shown on Fig. 11. In a first step, when $t \leqslant t_0$, α increases as a result of extension of existing debonds or of matrix cracking. Therefore the slope of the Ln$\dot{\varepsilon}$−Lnt curve is different from the time exponent $n=-0.8$.

In a second step when $t > t_0$, debonding is arrested, and α is constant. The slope of the Ln$\dot{\varepsilon}$−Lnt curve is now given by the time exponent $n=-0.8$.

Debonding during the first step is reflected by the elastic modulus decreases.

The above results also help in understanding the creep behaviour of the SiC/SiC composites. These composites exhibited a significant matrix cracking during static fatigue. As a consequence, α is time dependent, and the slope of the Ln$\dot{\varepsilon}$−Lnt curve is different from the time exponent $n=-0.8$. Therefore, creep of the SiC/SiC composites is controlled by matrix damage and creep of fibers.

4.4. Effect of cyclic loading

An equation similar to (9) can be obtained under cyclic loading by considering the average creep rate during a cycle:

$$\dot{\varepsilon}_p(t) = \frac{1}{2T}\int_t^{t+2T} \dot{\varepsilon}\,\mathrm{d}t \tag{12}$$

where $2T$ is the period of the sine type loading function:

Table 6
Comparison of α_1 and α_2 obtained for cyclic loading tests

ε_0 (%)	σ (MPa)	α_1 [Eq. (15)]	α_2 [Eq. (10)]
0.1	60	0.33	0.20
0.25	130	0.30	0.31
0.25	150	0.31	0.61

$$\sigma = \sigma_a + \Delta\sigma \sin(\pi t/T) \tag{13}$$

where σ_a is an average applied stress and $\Delta\sigma$ is the stress amplitude. When T is small compared to t, $t^{-0.8}$ can be considered to be constant during a cycle. Eq. (12) reduces to:

$$\dot{\varepsilon}_p = \frac{\alpha B_f}{2T}\left(\frac{2}{V_f}\right)^2\left(\frac{t}{t_0}\right)^{-0.8}\int_o^{2T}\sigma^2 dt \tag{14}$$

Inserting the expression of σ Eq. (13) into Eq. (14) and then integrating gives:

$$\dot{\varepsilon}_p = \alpha B_f\left(\frac{2}{V_f}\right)^2\left(\frac{t}{t_0}\right)^{-0.8}\sigma_p^2 \tag{15}$$

where $\sigma_p^2 = \sigma_a^2 + \frac{\Delta\sigma^2}{2}$ represents the equivalent creep stress actually carried by the fibers.

It can be noticed that the time exponent is again -0.8. This result agrees with the trend shown in Fig. 11. Furthermore, the same conclusions as above in static fatigue can be drawn using Eq. (15) for the creep behaviour in cyclic fatigue. This result supports the similarity in the creep mechanisms under static and cyclic fatigue that was indicated by experimental results.

Table 6 compares the α values estimated respectively from the composite creep behaviour [Eq. (15)] and from the elastic modulus change given by Eq. (10). The same trend as previously in static fatigue can be noticed. However there is a certain discrepancy for that specimen which had been tested under 150 MPa. This particular specimen exhibited the largest modulus decrease and matrix cracks within the longitudinal tows, whereas the creep behaviour was comparable to that of the other specimen with similar initial damage ($\varepsilon_0 = 0.25\%$) (Table 2 and Fig. 10). The origin of this matrix crack extension during fatigue tests has not been elucidated.

5. Conclusions

The creep behaviour of a SiC/Si-B-C composite during static or cyclic fatigue has been investigated at 1200 °C in argon. The tests were performed on specimens with a wide range of initial damage whose extent was controlled through magnitude of the deformation applied during a first cycle of loading at the test temperature.

The SiC/Si-B-C composite exhibited primary creep only, even during long tests (duration exceeding 85 h). Creep of the composite was found to be caused by creep of the Nicalon fibers, whatever the extent of initial damage. In those specimens with a saturated matrix damage ($\varepsilon_0 \geqslant 0.8\%$) the fibers are completely debonded from the matrix, and the load is carried essentially by the longitudinal fibers. When $0.3\% \leqslant \varepsilon_0 < 0.8\%$, the fibers are partially debonded from the matrix. When $\varepsilon_0 < 0.3\%$, the initial damage consists of cracks located within the intertow matrix and in the transverse tows, that may reach the longitudinal tows, but there are no cracks within the longitudinal tows. In these latter specimens with a limited damage, creep of the intratow matrix within the longitudinal tows also probably occurred, whereas the longitudinal tows were significantly debonded from the intertow matrix.

The time exponent in the creep rate expression was identical to that of fibers when the debond length is constant (-0.8). The stress exponent (2) is similar to that of stable fibers. The extent of initial damage determines the total debond length and the creep rate. Matrix damage remains constant when the initial damage involves transverse cracks in the longitudinal tows ($\varepsilon_0 > 0.3\%$). Limited elastic modulus decreases were measured on those specimens which did not contain cracks in the longitudinal tows. They were attributed to extension of tow debonds.

The creep behaviour of the SiC/Si-B-C composite is at variance with that of SiC/SiC composites in which both fiber creep and matrix cracking contribute to creep of the composite. The SiC matrix is creep resistant and stiffer than the Si-B-C matrix.

Acknowledgements

The authors gratefully acknowledge the support of SNECMA Moteurs and CNRS. The authors also wish to thank E. Pestourie and E. Inghels for valuable discussions, SNECMA for the production of samples, B. Humez for assistance with mechanical tests, J. Forget and C. Dupouy for manuscript preparation.

References

1. Lamouroux, F., Pailler R., Naslain, R. and Cataldi, M., French Patent no. 95 14843 (1995).
2. Carrère, P., *Thermostructural Behavior of a SiC/SiC Composite*, PhD thesis no. 1592 (1996), University of Bordeaux 1.
3. Forio, P., *Thermostructural Behaviour and Lifetime of a 2D Woven SiC/Si-B-C Composite with a Self Healing Matrix*. PhD Thesis no. 2171 (2000), University of Bordeaux 1.
4. Carrère, P. and Lamon, J., The fatigue behaviour at high temperature of a ceramic matrix composite with a self healing matrix. In *Proc. 8th International Spring Meeting, International Con-*

ference on Fatigue of Composites, ed. S. Degallaix, C. Bathias and R. Fougères. SF2M, 74–81 (1997).
5. Forio, P. and Lamon, J., Fatigue behaviour at high temperatures in air of a 2D SiC/Si-B-C composite with a self-healing multilayered matrix. *Ceramic Transactions American Ceramic Society*, Vol. 128, 2001, pp. 127–141.
6. Henager, C. H. and Jones, R. H., High-temperature plasticity effects in bridged cracks and subcritical crack growth in ceramic matrix composites. *Mat. Sci. Eng.*, 1993, **A166**, 211–220.
7. Holmes, J. W., Park, Y. H. and Jones, J. W., Tensile creep and creep recovery behaviour of a SiC-fiber-Si_3N_4-matrix composite. *J. Am. Ceram. Soc.*, 1993, **76**, 1281–1293.
8. Lamouroux, F., Steen, M. and Valles, J. L., *J. Eur. Ceram. Soc.*, 1994, **14**, 529–537.
9. Abbé, F., *Flexural Creep Behavior of a 2D SiC/SiC Composite*. PhD thesis, University of Caen, 1990.
10. Holmes, J. W. and Chermant, J. L., Creep behaviour of fiber reinforced ceramic matrix composites. In *High Temperature Ceramic Matrix Composites*, ed. R. Naslain *et al.* Woodhead, UK, 1993, pp. 633–647.
11. Abbé, F., Vicens, J. and Chermant, J. L., Creep behaviour and microstructural characterization of a ceramic matrix composite. *J. Mater. Sci. Lett.*, 1989, **8**, 1026–1028.
12. Evans, A. G. and Weber, C., Creep damage in SiC/SiC composites. *Mater. Sci. Eng.*, 1996, **A208**, 1–6.
13. Courtright, E., Engineering property limitations of structural ceramics and ceramic composites above 1600 °C. *Ceram. Eng. Sci. Proc.*, 1991, **12**, 1725–1744.
14. Bodet, R., Lamon, J., Jia, N. and Tressler, R., Microstructural stability and creep behaviour of Si-C-O (Nicalon) fibers in carbon monoxide and argon environment. *J. Am. Ceram. Soc.*, 1996, **79**(10), 2673–2686.
15. Guillaumat, L. and Lamon, J., Multiple cracking in 2D woven SiC/SiC composites. In *Microstructrure, Comportements Thermomécaniques et Modélisation des Composites Céramique-Céramique à Fibres*, ed. J. L. Chermant and G. Fantozzi. Revue des Composites et des Matériaux Avancés, Vol. 3, numéro hors série, 1993, pp. 159–171.
16. Guillaumat, L. and Lamon, J., Comportement mécanique et endommagement de composites à matrice céramique et renfort tissé (Mechanical behaviour and damage of woven ceramic matrix composites). *Revue des Composites et des Matériaux Avancés*, 1999, **9**(2), 183–203.
17. Bodet, R., Bourrat, X., Lamon, J. and Naslain, R., Tensile creep behaviour of a silicon carbide-based fiber with a low oxygen content. *J. Mater. Sci.*, 1995, **30**, 661–677.
18. Carter, C., Davis, R. and Bentley, J., Kinetics and mechanisms of high temperature creep in silicon carbide II. Chemically vapor deposited. *J. Am. Ceram. Soc.*, 1984, **67**(11), 732–740.
19. Di Carlo, J. and Yun, H., Creep and rupture behaviour of advanced fibers. In *Proc. ICCM 10, Vol. VI, Vancouver, British Columbia*, ed. A. Poursartip and K. Street. Woodhead Publishing Limited, Vancouver, BC, 1995, pp. 315–322.
20. Rugg, K., Tressler, R. E., Bakis, C. E. and Lamon, J., Creep of SiC-SiC microcomposites. *J. Eur. Ceram. Soc.*, 1999, **19**, 2285–2296.